BIOCHEMISTRY
including biophysical chemistry & molecular biology

Article

pubs.acs.org/biochemistry

Structure, Function, and On−Off Switching of a Core Unit Contact between CheA Kinase and CheW Adaptor Protein in the Bacterial Chemosensory Array: A Disulfide Mapping and Mutagenesis Study

Andrew M. Natale, Jane L. Duplantis, Kene N. Piasta, and Joseph J. Falke*

Department of Chemistry and Biochemistry and Molecular Biophysics Program, University of Colorado, Boulder, Colorado 80309-0596, United States

ABSTRACT: The ultrasensitive, ultrastable bacterial chemosensory array of *Escherichia coli* and *Salmonella typhimurium* is representative of the large, conserved family of sensory arrays that control the cellular chemotaxis of motile bacteria and Archaea. The core framework of the membrane-bound array is a lattice assembled from three components: a transmembrane receptor, a cytoplasmic His kinase (CheA), and a cytoplasmic adaptor protein (CheW). Structural studies in the field have revealed the global architecture of the array and complexes between specific components, but much remains to be learned about the essential protein−protein interfaces that define array structure and transmit signals between components. This study has focused on the structure, function, and on−off switching of a key contact between the kinase and adaptor proteins in the working, membrane-bound array. Specifically, the study addressed interface 1 in the putative kinase−adaptor ring where subdomain 1 of the kinase regulatory domain contacts subdomain 2 of the adaptor protein. Two independent approaches, disulfide mapping and site-directed Trp and Ala mutagenesis, were employed (i) to test the structural model of interface 1 and (ii) to investigate its functional roles in both stable kinase incorporation and receptor-regulated kinase on−off switching. Studies were conducted in functional, membrane-bound arrays or in live cells. The findings reveal that crystal structures of binary and ternary complexes accurately depict the native interface in its kinase-activating on state. Furthermore, the findings indicate that at least part of the interface becomes less closely packed in its kinase-inhibiting off state. Together, the evidence shows the interface has a dual structural and signaling function that is crucial for incorporation of the stable kinase into the array, for kinase activation in the array on state, and likely for attractant-triggered kinase on−off switching. A model is presented that describes the concerted transmission of a conformational signal among the receptor, the kinase regulatory domain, and the adaptor protein. In principle, this signal could spread out into the surrounding array via the kinase−adaptor ring, employing a series of alternating frozen−dynamic transitions that transmit low-energy attractant signals long distances.

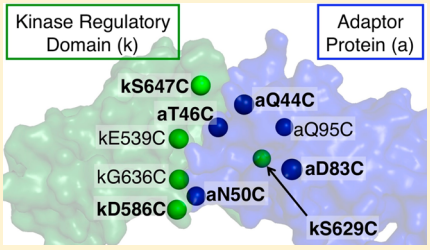

The bacterial chemosensory array directs cellular chemotaxis in attractant and repellent gradients, directing cellular migration toward an optimal living environment,[1−3] including the migration of certain pathogens during wound seeking and infection.[4−6] This sensory array exhibits a well-conserved architecture in motile bacteria and Archaea, and elements of the signaling mechanism are likely conserved, as well.[7,8] The exquisitely sensitive array can respond to a few molecules of attractant and exhibits remarkable stability with a functional lifetime of weeks in isolated bacterial membranes.[9−12]

A structural understanding of array architecture has begun to emerge. Cryo-electron microscopy (Cryo-EM) studies have provided a global view of the native architecture in cells, and crystal structures have generated a molecular view of specific components and complexes between them.[8,13−21] The array is formed of a hexagonal lattice of receptor oligomers (trimers of homodimers), and this lattice is believed to be stabilized by interconnected, heterohexameric rings of His kinase (CheA) and adaptor (CheW) components, as illustrated in Figure 1. In current array models, each kinase−adaptor ring is formed from alternating copies of the kinase regulatory domain (CheA P5 domain) and the adaptor protein. Notably, the two ring components share a conserved fold: both the kinase regulatory domain and adaptor protein are constructed of dual SH3-like subdomains.[22,23] These SH3-like subdomains are similar to eukaryotic SH3 domains that serve as adaptors in receptor-based signaling complexes.[24]

A molecular understanding of the structure and function of the bacterial chemosensory array is directly relevant to the conserved sensory arrays of bacteria and Archaea. More broadly, the architectural and mechanistic concepts illustrated by the bacterial chemosensory array are likely relevant to a growing class of eukaryotic receptor arrays that play important roles in neurotransmission, the immune response, and other signaling pathways.[24−28]

To develop a full, working molecular model of the bacterial chemosensory array, it is crucial to define the structures of the individual protein−protein interfaces that define the array architecture, as well as the functional roles of each interface in array stability and signal transduction. This study focuses on the

Received: August 23, 2013
Revised: September 28, 2013
Published: October 3, 2013

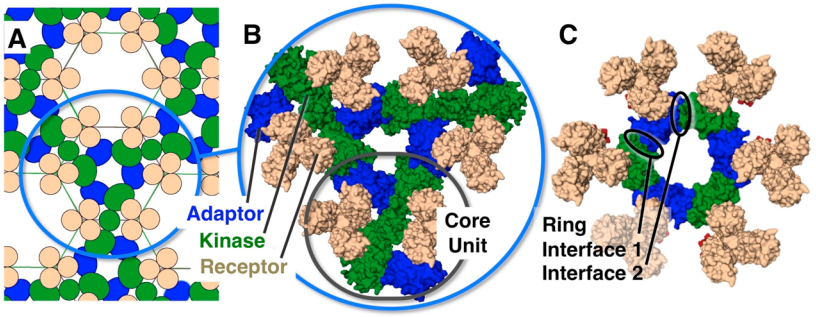

Figure 1. Structural model of the bacterial chemosensory array. (A) Schematic model showing the hexagonal lattice of receptor oligomers (trimers of dimers, tan) and the putative interconnected kinase−adaptor rings (the dimeric CheA kinase is colored green and the monomeric CheW adaptor protein blue).[34] (B) Crystal structure-based (PDB entry 4JPB[29]) threaded model of one ring formed by the association of three core units, each composed of two receptor oligomers, one kinase dimer, and two adaptor proteins. (C) Same, but nonring kinase domains have been omitted to highlight the heterohexameric ring formed by the structurally homologous kinase regulatory domain (KRD) and the adaptor protein. Also shown are the locations of representative KRD−adaptor interfaces 1 and 2 within the ring. These interfaces are located within and between core units, respectively. All molecular graphics were generated with PyMOL (PyMOL Molecular Graphics System, Schrödinger LLC).

first of two types of interfaces proposed to alternate in the heterohexameric kinase−adaptor ring. The targeted contact, termed "interface 1", is defined as the contact between subdomain 1 of the kinase regulatory domain and subdomain 2 of the adaptor protein (Figure 1). Two crystal structures have provided similar views of the interface at 3.5 Å (PDB entry 2CH4) and 3.2 Å (PDB entry 4JPB) resolution.[15,29] Chemical and genetic analyses support the existence of the interface in native arrays,[30−32] but the spatial resolution of these methods is more limited. The goals of the present study are (i) to test the crystallographic model (PDB entry 4JPB) of the interface in the functional, membrane-bound array and (ii) to investigate its functional roles in incorporation of the stable kinase into the array and in receptor-regulated kinase on−off switching. The experimental approach employs disulfide mapping[33] as well as site-directed Trp and Ala substitutions.[34] Together, these independent approaches reveal that the crystallographic model (PDB entry 4JPB) accurately depicts the structure of the interface in its kinase-activating "on state". Furthermore, the findings provide evidence that at least part of the interface becomes less closely packed in the off state, and that the interface has a dual structural and signaling function crucial both for incorporation of the stable kinase into the array and for kinase activation in the array on state. When combined with previous results, the findings suggest a simple model for concerted signal transmission among the receptor, the kinase regulatory domain, and the adaptor protein.

MATERIALS AND METHODS

Materials. All chemicals were highly pure reagent-grade. Chemicals were obtained from Sigma-Aldrich with the following exceptions. [γ-^{32}P]ATP was from Perkin-Elmer, DTT from Research Products International, and Ni-NTA agarose resin from Qiagen. Bicinchoninic acid assay (BCA) reagents were from Bio-Rad. PVDF was from Millipore. ECF Western blotting substrate was from GE Healthcare Life Sciences.

Protein Expression and Purification. *Salmonella typhimurium* CheA kinase and CheW adaptor protein possessing six-His tags on their N-termini were expressed by plasmids pET6H-CheA and pET6H-CheW, respectively, in *Escherichia coli* strain BL21(DE3) (Stratagene).[30] *E. coli* CheY with a C-terminal six-His tag was expressed by plasmid pVS-CheY-6H in *E. coli* strain plasmid M15-pREP4 (Qiagen).[35] CheA, CheW, and CheY proteins were isolated as previously described using standard Ni-NTA agarose affinity chromatography.[30,35] Protein concentrations were estimated by UV absorption using extinction coefficients calculated from protein sequences as previously described.[34] CheA kinase was obtained in ≥90% purity and CheW adaptor protein in ≥70% purity in all instances.

E. coli serine receptor (Tsr) was overexpressed by plasmid pJC3 in *E. coli* strain UU1581 that lacks all chemotaxis proteins, including receptors and adaptation enzymes.[36] Inside out, inner bacterial membrane vesicles containing Tsr were isolated as previously described.[30,37,38] The total membrane protein concentration was determined by the BCA assay; the fraction of total protein represented by receptors was determined by ImageJ densitometry of SDS−PAGE gels, and then the receptor concentration was determined by multiplying these two values.

The indicated CheA kinase and CheW adaptor protein point mutants were introduced into a cysteine-less background using the polymerase chain reaction-based QuickChange XLII mutagenesis kit (Agilent). All mutants were confirmed by DNA sequencing the coding region.

Reconstitution of Functional Signaling Arrays. Arrays were reconstituted as previously described[9,10,34] with minor modifications by combining 6.7 μM *E. coli* Tsr in inner membranes, 5 μM *S. typhimurium* CheA kinase, and 10 μM *S. typhimurium* CheW adaptor protein in 1× cross-linking buffer [160 mM NaCl, 6 mM $MgCl_2$, 3 mM EDTA, and 50 mM Tris (pH 7.5)] with 0.5 mg/mL BSA, 2 mM PMSF, and 2 mM TCEP. This mixture was incubated for 45 min at 22 °C, after which membranes with bound components were washed by pelleting at 21000*g* for 7 min at 4 °C, followed by resuspension of the pellets in 10 times their original volume of 1× cross-linking buffer with 1 mM PMSF and then repelleting and resuspending once again, and then finally resuspended in half their original volume of 1× cross-linking buffer with 1 mM PMSF (to an approximate receptor concentration of 13.4 μM). The chemotaxis proteins of *S. typhimurium* and *E. coli* are functionally interchangeable, and membrane-bound arrays generated using the components specified above are active and regulated by receptor attractant binding.[3,9,10,34]

Quantitation of Attractant-Regulated Kinase Specific Activity. Relative kinase activities of arrays were determined as previously described with some modifications.[30,34] Kinase

dx.doi.org/10.1021/bi401159k | *Biochemistry* 2013, 52, 7753−7765

reaction mixtures contained the following components at the indicated final concentrations in a total volume of 10 μL: washed arrays with approximately 3.4 μM Tsr with bound CheA and CheW, 50 μM CheY, 1× cross-linking buffer with additional 2 mM $MgCl_2$, and 1 mM [γ-^{32}P]ATP (0.1−0.2 mCi/mL). Attractant sensitivity was tested by including 2 mM serine in the reaction mixture. Reactions were initiated by the addition of ATP, allowed to proceed for 10 s, and then quenched by the addition of 30 μL of 2× Laemmli sample buffer containing 40 mM EDTA. The resulting samples were resolved on denaturing SDS−PAGE gels, which were then dried, and the CheY−$^{32}P_i$ band was imaged using a phosphorimager system and quantitated using ImageJ.

To determine specific activity, an additional portion of each washed array sample was resolved on reducing, 10% acrylamide SDS−PAGE gels that were then stained with Coomassie Brilliant Blue R-250 and imaged using a FluorChem HD2 imager, and the CheA kinase band density was quantitated using ImageJ to determine relative kinase concentrations in each sample. Relative CheY−$^{32}P_i$ levels were divided by relative CheA kinase concentrations to determine a specific kinase activity for each tested array.

Free CheA Kinase Assay. The autokinase activity of free CheA was determined as previously described, with some modifications.[30] Autokinase reaction mixtures contained the following components at the indicated final concentrations in a total volume of 10 μL: 20 μM CheA, 50 μM CheY, 1× cross-linking buffer with additional 2 mM $MgCl_2$, and 1 mM [γ-^{32}P]ATP (0.2−0.4 mCi/mL). Reactions were initiated by the addition of ATP, allowed to proceed for 20 s, and then quenched, and the products were analyzed in the same way as in reconstituted array kinase activity assays (described above).

Disulfide Mapping Oxidation Reactions. Oxidation reactions were performed as previously described with minor modifications.[34] Reconstituted arrays prepared as described above were oxidized by the addition of Cu(II) (in the form of $CuCl_2$) in 1× cross-linking buffer. All reaction mixtures contained 3 mM EDTA to buffer the Cu(II), ensuring a low concentration of free Cu(II) and mild oxidation conditions.[34] Final samples contained washed arrays at a Tsr concentration of 3−5 μM, with final Cu(II) concentrations ranging from 1 to 5 mM for standard cross-linking experiments or from 0.6 to 1.2 mM for experiments that aimed to examine the effects of serine or isoleucine on reaction rate. In the latter experiments, serine and isoleucine were added to reaction mixtures at concentrations of 0.5 mM, and Cu(II) concentrations were tuned to a particular value for each type of array being tested. Reactions were initiated by the addition of the Cu(II) and then quenched by the addition of twice the reaction volume of 2× Laemmli sample buffer with 6.7% SDS, 40 mM EDTA, and 80 mM *N*-ethylmaleimide, either 10 s after the addition of Cu(II) (in the case of standard oxidation reactions) or 8 s afterward (in the case of Ser/Ile effect experiments). All reactions were conducted at 22 °C. Samples were then incubated at 98 °C for 60 s, snap-frozen in liquid N_2, and stored at −80 °C.

Quantitation of the Disulfide-Linked CheA Kinase−CheW Adaptor Heterodimer. Cross-linked products of oxidation reactions were monitored by Western blotting using a polyclonal primary antibody against CheA kinase (kindly provided by J. Stock) and the anti-rabbit, alkaline phosphatase-conjugated secondary antibody (Sigma), as previously described.[34] Briefly, diluted samples were resolved by SDS−PAGE and transferred to PVDF membranes by electroblotting. Tris-buffered saline with 0.05% (v/v) Tween 20 and 3% (w/v) dry milk powder was used for blocking membranes and for all antibody dilutions. Washes were performed using Tris-buffered saline with 0.05% (v/v) Tween 20. Washed membranes were developed by incubation with the ECF substrate, dried, and imaged with a Typhoon 9400 scanner. Blots were quantified by densitometry using ImageJ.

TAM-IDS. *In vivo* TAM-IDS experiments were conducted as previously described with some modifications.[34] Plasmids pSF2 and pSF5 encoding N-terminal YFP fusions of the *E. coli* CheA CheY/B binding domain (P2) and kinase regulatory domain (P5), respectively, were transformed in RP9535 (ΔcheA) cells, and single colonies were grown overnight at 30 °C in VBC minimal growth medium supplemented with HMLTT containing 0.75% glycerol and 100 μg/mL ampicillin.[39] The overnight culture was diluted 10-fold into fresh VBC medium and grown until midlog phase (OD_{600} between 0.04 and 0.09). Induction was initiated by the addition of fresh 50 μM IPTG and allowed to proceed for 2 h. The cells in 10 mL of culture were collected by centrifugation for 5 min at 3200*g* and resuspended in 700 μL of imaging buffer [10 mM potassium phosphate, 0.1 mM EDTA, 1 mM L-methionine, and 10 mM sodium lactate (pH 7.0)].[40] The cells were then repelleted and resuspended in a final volume of 20 μL of imaging buffer. Finally, 20 μL of washed cells was pipetted onto a thin agarose pad (1% agarose in imaging buffer) and allowed to set for 3 min before a coverslip was added. Cells were immediately imaged on a Nikon TE-2000-E inverted microscope utilizing a 60× oil immersion objective, CFP/YFP/RFP dichroic mirror with corresponding single-band excitation and emission filters, and a CoolSNAP ES camera with an exposure time of 600 ms. Excitation was provided by a mercury lamp.

TAM-IDS was applied *in vitro* as previously described.[34] Briefly, Ala and Trp mutants were constructed in the Cys-less CheA kinase background using site-directed mutagenesis as described above, and the effect of the mutations on stable CheA kinase incorporation and specifc activity was measured in reconstituted arrays. Stable CheA kinase incorporation is defined as the density ratio of CheA kinase to receptor, visualized on Coomassie gels, and measured with ImageJ as previously described.[10] *In vitro* kinase assays were performed as described above.

Assaying the Specific Kinase Activity of Disulfide-Linked CheA Kinase. To generate arrays containing stably incorporated, disulfide-linked CheA and CheW, a reconstitution procedure slightly modified from that described above was used. Array components were mixed under the same conditions as described above, except that no reducing agent was added to the mixture. The mixture was incubated at 22 °C for 45 min and then oxidized by the addition of 5 mM Cu(II) in the form of $CuCl_2$. Oxidized arrays were then washed, aliquoted, and assayed for (i) incorporation of kinase into the array, (ii) the extent of disulfide-linked heterodimer formation, and (iii) specific kinase activity as described above.

Statistics. Error bars are reported as standard errors for the indicated values of *n*. Tests of statistical significance employed the independent, nondirectional Student's *t* test for unpaired variables.

RESULTS

Construction of a Working Model of the Kinase Regulatory Domain−Adaptor Protein Interface. The current structural model for kinase−adaptor interface 1 is

based on a complex between *Thermotoga maritima* components, including a receptor cytoplasmic domain fragment, a CheA kinase fragment possessing the dimerization (P3), catalytic (P4), and regulatory domains (P5), and the CheW adaptor protein (PDB entry 4JPB[29]). The *T. maritima* components have proven to be especially well suited for structural studies.[8,13−19,21] For functional studies, reconstituted arrays constructed from *E. coli* and *S. typhimurium* components are especially useful and display both sequence and structural homology with *T. maritima* arrays and components.[7−10,30,34,35,41−49] Herein, a proven reconstituted array composed of the natively Cys-less *E. coli* serine receptor and Cys-less constructs of the *S. typhimurium* kinase and adaptor proteins was selected for analysis. This proven array is known to exhibit high kinase activity, full regulation by attractant, and ultrastability *in vitro*.[9,10,34] To model the structure of this complex, the protein sequences of *S. typhimurium* components were threaded onto the most recent, highest-resolution crystal structure of the *T. maritima* complex (PDB entry 4JPB[29]) using the Phyre2 protein modeling server.[50] Panels B and C of Figure 1 present the working structural model.

The goals of the study were (i) to test the validity of the interface 1 structural model by disulfide mapping and mutational analysis and (ii) to investigate the nature of on−off switching at this interface via the effects of attractant signals on disulfide formation rates, and via the effects of interfacial disulfides and side chain substitutions on function. Studies were conducted on reconstituted, functional arrays assembled on *E. coli* membranes containing native receptors by mixing the isolated membranes with purified kinase and adaptor protein, incubating to allow self-assembly, and then washing to remove unbound components as previously described.[9,10,34]

Testing the Structural Model through Disulfide Mapping. Disulfide mapping techniques have proven to be useful as a tool for studying protein−protein interactions in signaling proteins.[33,34,48,49,51] Cys substitutions are generally nonperturbing at surface positions and are introduced in target proteins with single-site precision. The rate of the disulfide bond formation reaction between solvent-exposed Cys residues is sensitive to the proximity of the two residues, as well as to their geometry, dynamics, and environment.

Surface-exposed positions were selected for Cys mutations, yielding five kinase and five adaptor protein single-Cys mutants, as summarized in Figure 2 and Table 1. Each Cys mutation was located at the periphery of the predicted interface 1 to maximize its accessibility to oxidation chemistry. After purification via standard methods, each Cys mutant was tested for function in reconstituted arrays, as outlined in Figure 3. Mutants yielding <50% normal array incorporation or kinase activity, relative to that of the corresponding Cys-less protein, were rejected. Altogether, three kinase and four adaptor protein single-Cys mutants retained function and were utilized for disulfide mapping.

The surviving single-Cys mutants were used to generate reconstituted arrays containing a pair of Cys residues, one on the kinase and the other on the adaptor protein, yielding a different reconstituted array for each of the 12 possible pairwise combinations. Table 2 presents the specific kinase activities of the 12 arrays, each of which retained at least 50% of the specific kinase activity relative to Cys-less and were fully downregulated by serine binding. The crystal structure-based threaded model predicts a wide range of C_β−C_β separation distances within the set of mutant pairs, from 6.9 Å for the closest pair to 29.7 Å for the most distant.

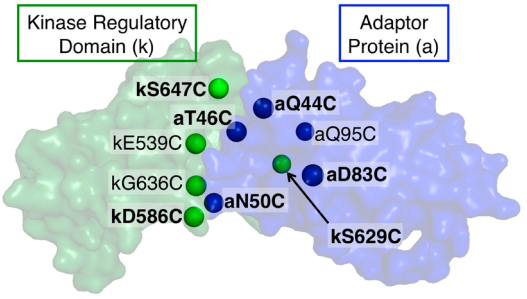

Figure 2. Crystal structure-based (PDB entry 4JPB[29]) threaded model of kinase−adaptor interface 1, illustrating engineered Cys positions. Shown are the adaptor protein CheW (blue) and the kinase regulatory domain of CheA (green), with β-carbons of the 10 starting engineered Cys positions depicted as spheres. Both of the *T. maritima* proteins in the crystal structure were threaded with the sequences of the *S. typhimurium* proteins used in our experimental studies (see Results). The seven Cys mutations found to form functional arrays and employed in subsequent disulfide mapping studies are highlighted by bold labels.

Table 1. Kinase and Adaptor Protein Single-Cys Mutants

single-Cys mutant[a] (*T. maritima* residue)	secondary structure	stable kinase incorporation in arrays (% of Cys-less)	specific kinase activity in arrays: without Ser (% of Cys-less)	specific kinase activity in arrays: with Ser (% of Cys-less)
kE539C (L554)	β-strand	80 ± 5	20 ± 10	0 ± 10
kD586C (Q600)	loop	110 ± 5	80 ± 10	10 ± 10
kS629C (K642)	loop	95 ± 10	80 ± 10	10 ± 10
kG636C (E649)	loop	80 ± 5	20 ± 10	0 ± 10
kS647C (S660)	β-strand	90 ± 5	70 ± 10	10 ± 10
aQ44C (D38)	loop	85 ± 5	70 ± 10	10 ± 10
aT46C (T40)	loop	95 ± 5	80 ± 20	10 ± 10
aN50C (K44)	loop	70 ± 5	60 ± 20	10 ± 10
aD83C (K77)	loop	90 ± 5	120 ± 20	10 ± 10
aQ95C (D88)	loop	40 ± 10	20 ± 10	0 ± 10

[a]Shown are equivalent residues for the His kinase (CheA) and adaptor (CheW) proteins of *S. typhimurium* and *T. maritima*, where prefixes k and a indicate kinase and adaptor protein, respectively.

To generate a map of protein−protein interactions across the interface, we subjected each of the 12 reconstituted, washed arrays containing different Cys pairs to oxidizing conditions and measured the rate of kinase−adaptor protein disulfide formation. Arrays were reconstituted and washed in the same manner as in kinase activity assays, and oxidation reactions were conducted in the same physiological buffer as in kinase activity assays. Oxidation of Cys pairs to disulfides with ambient dissolved oxygen was initiated by adding the catalyst Cu(II) buffered with EDTA. Initially, three different oxidation strengths were used: 1, 2, and 5 mM Cu(II), each buffered in 3 mM EDTA. The first two systems buffered with excess EDTA [termed Mild (I) and Mild (II)] yielded subnanomolar levels of free Cu(II), while the third system (Moderate) yielded 2 mM free Cu(II).[52] Notably, these reaction mixtures lacked 1,10-

dx.doi.org/10.1021/bi401159k | *Biochemistry* 2013, 52, 7753−7765

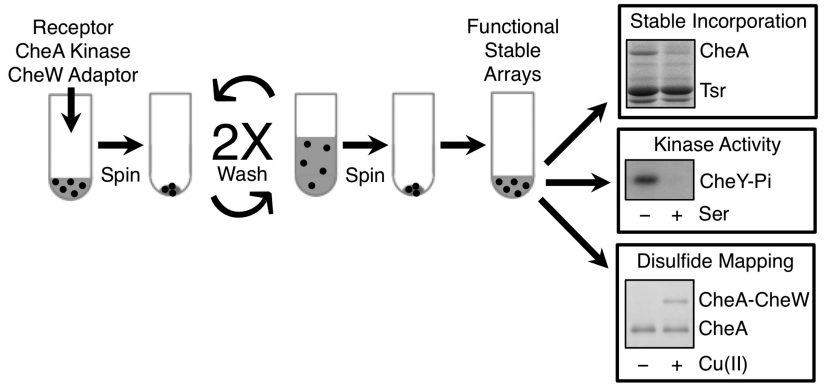

Figure 3. Protocol for *in vitro* array assembly and representative experimental data. Functional, membrane-bound arrays were reconstituted *in vitro* by combining purified *S. typhimurium* CheA kinase and CheW adaptor protein with *E. coli* serine receptor purified in bacterial inner membranes.[9,10,34] Incubation allows arrays to self-assemble, and then washing to remove unbound proteins yields functional, ultrastable, membrane-bound arrays to be used in experiments. Also shown are representative experimental data obtained in (i) the kinase incorporation in the presence and absence of adaptor protein, respectively, (ii) the kinase activity assay, and (iii) the disulfide mapping assay.

Table 2. Function-Retaining Cys Mutant Pairs

kinase–adaptor mutant pair	modeled C_β–C_β separation (Å)	stable kinase incorporation in arrays (% of Cys-less)	specific kinase activity in arrays: without Ser (% of Cys-less)	specific kinase activity in arrays: with Ser (% of Cys-less)
kD586C–aQ44C	21.7	95 ± 10	70 ± 10	0 ± 10
kD586C–aT46C	15.8	100 ± 5	90 ± 20	10 ± 10
kD586C–aN50C	6.9	100 ± 10	100 ± 20	10 ± 10
kD586C–aD83C	24.6	100 ± 5	100 ± 20	10 ± 10
kS629C–aQ44C	22.2	80 ± 15	50 ± 10	10 ± 10
kS629C–aT46C	17.7	85 ± 10	60 ± 20	10 ± 10
kS629C–aN50C	16.6	65 ± 10	60 ± 10	0 ± 10
kS629C–aD83C	29.7	90 ± 15	100 ± 30	10 ± 10
kS647C–aQ44C	9.0	85 ± 15	80 ± 20	10 ± 10
kS647C–aT46C	7.8	90 ± 15	80 ± 10	10 ± 10
kS647C–aN50C	20.2	50 ± 5	80 ± 20	10 ± 10
kS647C–aD83C	24.4	75 ± 5	110 ± 20	10 ± 10

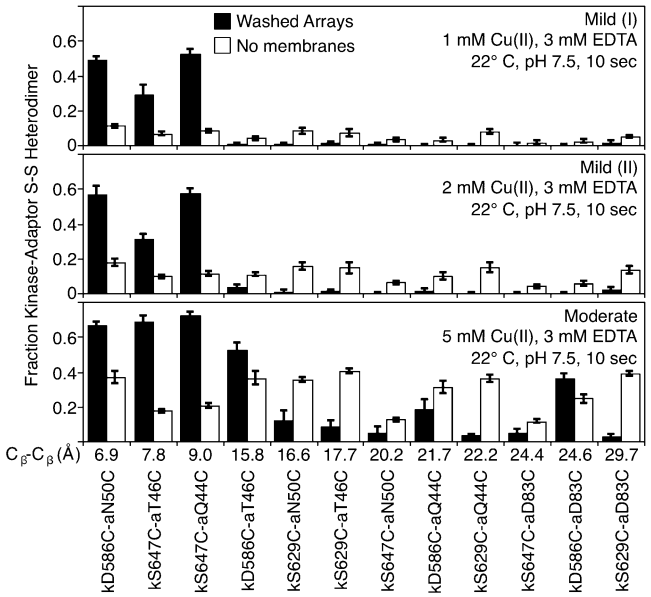

Figure 4. Relative disulfide formation extents for functional Cys pairs in reconstituted arrays, where the Cys pairs are arranged in order of increasing C_β–C_β separations as predicted by the crystal structure-based (PDB 4JPB[29]) threaded model. Disulfide formation reactions were conducted on reconstituted arrays containing the 12 functional Cys pairs (black bars). Reactions used three mild oxidation conditions [1, 2, and 5 mM Cu(II), each buffered with 3 mM EDTA]. Three of 12 pairs (kD586C–aN50C, kS647C–aQ44C, and kS647C–aT46C) exhibited substantially greater rates than the remaining nine pairs. Predicted C_β–C_β separations for the three fast pairs were all <10 Å, while separations for other pairs ranged from 15.8 to 29.7 Å. Disulfide formation reactions were also conducted on the free kinase and adaptor in solution without membranes, using the same oxidation conditions (white bars). Notably, the strong spatial dependence of disulfide formation rates observed in the array is lost in solution. The standard error is shown for each reaction, where n = 3–12. C_β–C_β separations were measured with PyMOL (PyMOL Molecular Graphics System, Schrödinger LLC).

phenanthroline previously used in many studies to convert the redox catalyst Cu(II) into the stronger catalyst Cu(II)(1,10-phenanthroline)$_3$.[33] While the stronger catalyst was well suited to these previous studies, the milder, buffered Cu(II) catalyst was better suited to the current study that included a subset of very fast disulfide reactions.

Oxidation reactions were quenched after 10 s with 4% SDS, 50 mM *N*-ethylmaleimide (NEM), and 25 mM EDTA, and then the mixtures were subjected to SDS–PAGE followed by anti-CheA kinase Western blotting to detect the two major bands: kinase monomer and the disulfide-stabilized, kinase–adaptor protein heterodimer. Integration of the kinase monomer and heterodimer bands yielded the ratio of cross-linked kinase to total kinase, thereby quantifying the extent of disulfide formation. As anticipated for a disulfide cross-link, most or all (≥80%) of the heterodimer band was reversed back to the individual monomer bands by the reducing agent DTT (not shown).

Figure 4 (black bars) summarizes the resulting disulfide formation extents in washed arrays, where the Cys pairs are

dx.doi.org/10.1021/bi401159k | *Biochemistry* 2013, 52, 7753–7765

arranged in order of increasing C_β–C_β separations as predicted by the crystal structure-based threaded model. In reconstituted arrays under the two mildest oxidation conditions [1 or 2 mM Cu(II), with 3 mM EDTA as a buffer], only 3 of 12 cysteine pairs (kD586C–aN50C, kS647C–aQ44C, and kS647C–aT46C) exhibited significant reactivity, each yielding at least 25% conversion of the total kinase population to the heterodimer (Figure 4, black bars). Each of the nine other pairs yielded <4% conversion to the heterodimer under the same conditions (Figure 4). The three most reactive pairs are predicted to have the shortest C_β–C_β separations (6.9–9.0 Å), whereas the nine slower pairs are all predicted to be more distal (15.8–29.7 Å). Thus, the findings provide strong evidence that the crystal structure-based threaded model represents an accurate picture of the native interface as it exists in functional signaling arrays.

Notably, the three fastest disulfide formation reactions (Figure 4) were among the fastest we have observed in many studies.[33,34,48,49,51] This exceptional speed likely arises from an unusual combination of high proximity and geometry, a high level of exposure to the aqueous oxidation agent, and favorably local dynamics that produces rapid, productive collisions between the two Cys residues. These fast reactions approached completion even under the mildest conditions as indicated by the relative insensitivity of the reactions to the increasing concentration of the free Cu(II) catalyst (Figure 4). The increasing catalyst concentration in turn increases the concentrations of the oxidation agent reactants (superoxide anion and hydroxyl radical), although this increase is not linear with free Cu(II) because the dissolved dioxygen needed to form the oxidation agents is limited (~200 μM ambient O_2). At completion, the fast pairs yielded a maximal level of ~75% disulfide formation (Figure 4C, and confirmed by time courses); the remaining ~25% of the products are presumably oxidized sulfhydryls generated by a known competing reaction.[33] The disulfide reactions of the slower Cys pairs are considerably further from completion as indicated by their greater sensitivity to the Cu(II) concentration (Figure 4).

The clear spatial pattern of disulfide formation rates observed in reconstituted arrays under mild oxidation conditions, fast rates for proximal pairs and slow rates for distal pairs, differs significantly from the pattern seen for free kinase–adaptor pairs in solution. For comparison, the same buffer and catalyst conditions were applied to all mutant kinase–adaptor pairs in the absence of receptor-containing membranes (Figure 4, white bars). In these reactions, kinase and adaptor protein were present at total concentrations of 5 and 20 μM, respectively, to drive their association into soluble complexes. Because the soluble kinase and adaptor protein bind each other only transiently in the absence of a receptor lattice and are not locked into an array with a specific geometry, the resulting disulfide formation reactions were less selective. In solution, tumbling and random collisions allow detectable, nonspecific formation of disulfides even under mild oxidation conditions. By contrast, the greater spatial specificity exhibited by disulfide reactions in reconstituted arrays highlights the high degree of spatial order in the array.

Selection of a Library of Tryptophan and Alanine Mutants for TAM-IDS Analysis. To gain further insight into the structure and signaling function of the kinase–adaptor interface, we employed tryptophan and alanine mutagenesis to identify docking sites (TAM-IDS).[34] This approach substitutes both a larger and smaller side chain for a native residue, thereby generating both a bump and a hole on a given protein surface. Trp substitutions at a critical protein–protein interface would be expected to perturb binding and/or function, except in cases where they can rotate out of the contact region. Interfacial alanine mutations would not be expected to be perturbing, unless the native residue is essential. This leads to a natural classification of mutation sites into three categories: essential residues (both Trp and Ala are perturbing), interfacial residues (Trp is perturbing, and Ala is not), and noninterfacial–peripheral residues (neither Trp nor Ala is perturbing). Analysis of the observed pattern of these classified residues provides an independent method for checking an interface defined by disulfide mapping, and it can also provide information about interface function.

For this study, we selected four positions on the surface of the kinase regulatory domain to target for Trp and Ala substitutions (Figure 5A). Three of the positions (kN630,

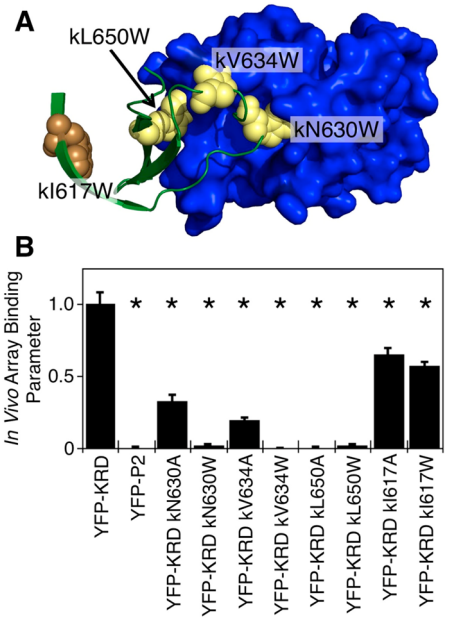

Figure 5. Quantitating the effects of Trp and Ala mutations on the incorporation of the kinase regulatory domain into live cell arrays (*in vivo* TAM-IDS). (A) Model of the four Trp mutations on the kinase regulatory domain selected for TAM-IDS analysis. Notably, all common conformers of kN630W, kV634W, and kL650W are predicted to clash with the blue adaptor protein, while none of the kI617W conformers are predicted to clash. (B) The isolated kinase regulatory domain was fused to YFP, and its ability to stably incorporate into the polar arrays of live cells lacking intrinsic CheA kinase was quantified by fluorescence microscopy as previously described.[34] The resulting array binding parameter ranges from unity for the native incorporation exhibited by the wild-type kinase regulatory domain (YFP-KRD) to zero for a negative control domain (YFP-P2). The standard error is shown for each binding reaction, where $n = \geq 30$ cells, quantified in three separate experiments. Asterisks indicate statistically significant losses of array incorporation relative to that of WT YFP-KRD ($p < 0.05$). For the sake of consistency with all other experiments herein employing the *S. typhimurium* kinase *in vitro*, the indicated position labels are for *S. typhimurium* residues. The corresponding *E. coli* residues (italicized) for the kinase regulatory domain employed in this *in vivo* experiment are as follows: kI617 = *kI600*, kN630 = *kN613*, kV634 = *kV617*, and kL650 = *kL633* (the *S. typhimurium* and *E. coli* kinase regulatory domains are nearly identical, differing by only 8 of 145 residues).

dx.doi.org/10.1021/bi401159k | *Biochemistry* 2013, 52, 7753–7765

kV634, and kL650) were predicted by the crystal structure-based threaded model to be within the packed area of the kinase−adaptor interface, whereas an additional position distal to the interface (kI617) was selected as a negative control. To conduct TAM-IDS *in vivo*, mutations were introduced at each target position in an isolated kinase regulatory domain fused to YFP. For *in vitro* analysis, each mutation was also introduced into full-length, Cys-less kinase.

Analyzing Interface Structure Using TAM-IDS in Live Cells. To further test the interface structure predicted by the crystal structure-based threaded model and the disulfide mapping results, we conducted TAM-IDS *in vivo* using the isolated kinase regulatory domain fused to YFP. Previous studies have demonstrated the ability of a similar construct to assemble into the chemosensory lattices of live cells, visible as localized fluorescent regions at the bacterial cell pole.[34,40] Here we assessed the ability of the mutant fusion proteins to assemble into arrays in cells lacking endogenous kinase. The quantitative method used to evaluate array binding measures the corrected array brightness of each cell in a population and then averages and normalizes the brightness over the population to generate a relative binding parameter ranging from 0 to 1, where 0 corresponds to the negligible array binding of a negative control [kinase CheY/B binding domain (P2) fused to YFP] and 1 represents the normal level of binding seen for the WT kinase regulatory domain (see ref 34 for a detailed description of the method).

Figure 5B shows the *in vivo* array binding parameter for the Ala and Trp mutants at each of the selected positions. The introduction of Trp substitutions at each of the three experimental positions greatly reduced the level of stable array incorporation, a result consistent with the model's prediction that all three residues exhibit significant burial at the kinase−adaptor interface. Bulky Trp substitutions at these positions would be expected to disrupt the packing interactions required for normal interface assembly, resulting in the observed loss of incorporation. Both Trp and Ala substitutions at position kL650 caused a virtually total loss of incorporation, indicating that the native Leu side chain is essential for interface assembly, tolerating neither bulky substitution nor truncation. Ala substitutions at the remaining interfacial positions (kN630 and kV634) exhibited significantly ($p < 0.05$) decreased levels of incorporation relative to that of WT while retaining some ability to bind. Thus, these native side chains are able to tolerate truncation to varying degrees. Although both substitutions at control residue kI617 decreased the level of incorporation relative to that of WT, perturbations were significantly less severe than at interfacial positions and were of the same magnitude for both Ala and Trp substitutions. It follows that this position is located largely outside the packing region of the interface, as predicted by the model.

Analyzing Interface Structure and Function in Reconstituted Arrays by TAM-IDS. The results of the disulfide mapping and *in vivo* TAM-IDS studies indicate that the crystal structure-based threaded model closely approximates the structure of the interface in the membrane-bound array. To gain insight into the function of the interface, we conducted TAM-IDS *in vitro* by incorporating the same set of Trp and Ala substitutions into the kinase regulatory domain of full-length, Cys-less kinase. The advantage of the *in vitro* assay is the ability to separately quantify both (i) stable kinase incorporation into the array and (ii) the specific activity of the incorporated kinase molecules. Such information can reveal the contribution of the interface to array assembly and to kinase activation, respectively.

All full-length *S. typhimurium* kinase mutants were expressed well and were stably purified, showing no tendency to aggregate. Each was reconstituted into washed arrays and then assayed for stable kinase incorporation and specific kinase activity, relative to those of positive control Cys-less kinase, as illustrated in Figure 6A. Interfacial Trp substitutions kN630W

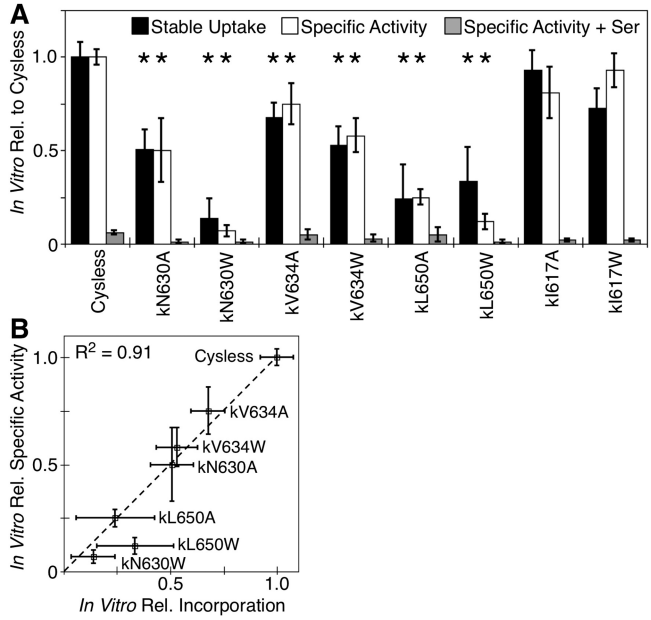

Figure 6. Quantitating the effects of Trp and Ala mutations on stable kinase incorporation and specific kinase activity in reconstituted arrays (*in vitro* TAM-IDS). (A) Reconstituted, membrane-bound arrays containing each of the indicated Trp and Ala mutations in the Cys-less kinase background were prepared. Stable kinase incorporation into the array (black bars) was normalized to the incorporation measured for Cys-less kinase. Specific kinase activity (white bars, measured as the ratio of the total kinase activity to the total amount of kinase in the array) was normalized to the specific activity of the Cys-less kinase in the absence of attractant. Specific activities in the presence of attractant (2 mM Ser) were determined in the same fashion. The standard error is shown for each bar, where $n = 5-15$. Asterisks indicate statistically significant changes relative to the value of the Cys-less form ($p < 0.05$). (B) Correlation plot of specific kinase activity vs stable kinase incorporation for the six interfacial Trp and Ala mutations (kI617W and kI617A omitted), and for the Cys-less form. The data are well-fit ($R^2 = 0.91$) by a perfect correlation model [$y = x$ (---)].

and kL650W decreased the level of incorporation to <50% of Cys-less levels, while Trp mutant kV634W retained approximately 50% incorporation. The only Ala substitution to reduce the level of incorporation to <50% was kL650A. Perturbations in specific kinase activity followed approximately the same trend, with mutants kN630W, kL650W, and kL650A exhibiting less than 50% of the specific activity of Cys-less kinase and mutants kN630A, kV634W, and kV634W being less perturbing. Notably, the observed kinase activities of all eight mutant CheA proteins were downregulated by the attractant serine, indicating that each modified array retained functional, attractant-triggered switching from the on state to the off state.

The high degree of perturbation to both stable incorporation and activity seen for Trp mutant kN630W, and to a lesser extent for mutants kL650W and kL650A, raised the question of

dx.doi.org/10.1021/bi401159k | *Biochemistry* 2013, 52, 7753−7765

whether any of the observed effects of mutations are due to perturbations of overall kinase folding rather than site specific effects on interface 1. As the purified, native kinase retains small but measurable autophosphorylation activity outside of arrays,[53,54] we measured the specific autokinase activity of each isolated mutant protein in the absence of membranes and adaptor protein to confirm that each retained essential kinase structure and function. All eight mutants, both Ala and Trp, retained ≥70% of the specific autokinase activity of Cys-less kinase. It follows that all retained native folding and domain structure and that the observed perturbations were specific to interface 1.

As previously observed in a TAM-IDS study of the interface between the receptor and the kinase regulatory domain,[34] interfacial mutations had a stronger impact on the array incorporation of the isolated kinase regulatory domain *in vivo* than on the array incorporation of full-length kinase *in vitro*. The greater sensitivity of the isolated domain to mutations was not surprising, because the full-length kinase is dimeric, and its other domains may contribute to array contacts. Thus, the more extensive contacts and larger binding free energy of the full-length kinase allow it to compensate for mutational perturbations better than the isolated domain. Taking into account the compensatory effects of this stabilization, we observed the same general pattern of relative effects for the interface perturbations in both the *in vivo* and *in vitro* TAM-IDS experiments, such that the Trp substitutions at positions kN630, kV634, and kL650 all caused larger perturbations than the control Trp substitution at position kI617. The Trp substitution at position kV634 was less perturbing than that at kN630 or kL650 *in vitro*, likely due to the fact that the kV634 position is located on a loop that could give the Trp side chain additional flexibility to snorkel out of the interface.

The *in vitro* TAM-IDS analysis indicates that the interface is important for both stable array assembly and kinase activation, suggesting the interface possesses both structural and signaling functions. In particular, quantitative analysis of the *in vitro* TAM-IDS data (Figure 6A) revealed a strong correlation between the effects of mutations on stable kinase incorporation into the array and on the specific activity of the incorporated kinase molecules, yielding an R^2 value of 0.91 in Figure 6B. By contrast, analysis of previously published data[34] for a different array interface yielded an R^2 value of only 0.12. Comparison of these remarkably different R^2 values highlights both (i) the special correlation between array incorporation and specific kinase activity at ring interface 1, indicating a strong link between its dual structural and signaling roles, and (ii) the lack of such a correlation at the receptor−kinase interface where the contact is more important for signaling than for array structure, as previously concluded.[34]

Probing On−Off Switching through Changes in Transinterface Disulfide Formation Rates. Because the formation of a given disulfide is sensitive to structural, dynamic, and environmental changes, it can be useful as a detector of local changes triggered by on−off switching.[33,55,56] Thus, arrays containing the three most rapidly reacting pairs identified in the disulfide mapping analysis (kD586C−aN50C, kS647C−aQ44C, and kS647C−aT46C) were oxidized in the presence and absence of the attractant serine. Reactions were conducted in a manner similar to that of the disulfide mapping experiments described above except that the oxidation strength of each reaction was empirically tuned by adjusting the Cu(II) concentration for each Cys pair (see the legend of Figure 7), to help ensure the reaction was sensitive to both increases and decreases in the reaction rate. In principle, the resulting tuned reactions would be able to detect attractant-triggered rate changes of either sign. Arrays were reconstituted and washed as usual, mixed with serine, buffer, or a control amino acid, and then subjected to the optimized oxidation reaction.

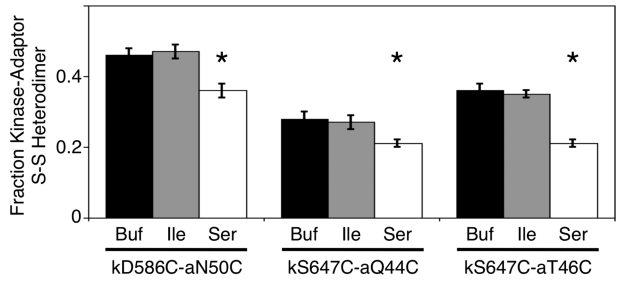

Figure 7. Effects of attractant-triggered signals on the relative disulfide formation rates of three engineered Cys pairs in reconstituted arrays. Shown are the reaction rates of the three fastest di-Cys pairs identified by disulfide mapping analysis (Figure 4), measured in the presence and absence of Ser and a control amino acid, Ile. Oxidation conditions were tuned for each pair to ensure the 8 s reaction remained sensitive to both increases and decreases in the reaction rate [the catalyst was 0.7, 0.6, and 1.2 mM Cu(II) in 3 mM EDTA for the kD586C−aN50C, kS647C−aQ44C, and kS647C−aT46C pairs, respectively]. Asterisks indicate statistically significant decreases in rate ($p < 0.05$), which were observed for all three pairs in the presence of 0.5 mM Ser (white bars) relative to buffer (black bars) or 0.5 mM Ile (gray bars). Reactions between the free kinase and adaptor mutant pairs in solution, conducted under the same oxidation conditions, exhibited no dependence on either Ser or Ile (data not shown). The standard error is shown for each bar, where $n = 7−16$.

For all three arrays, a small but consistently detected and highly significant ($p < 0.05$) decrease in reaction rate was triggered by the presence of serine, as shown in Figure 7. In contrast, this rate decrease was not observed upon addition of buffer, or a control amino acid (isoleucine). It follows that attractant-triggered, receptor-mediated, array on−off switching alters the structure or dynamics of this interface.

Testing the Effects of Transinterface Disulfide Bonds on Array Function. To further examine the structure and function of the interface, we next examined the effect of preformed, interface-spanning disulfide bonds on receptor-regulated kinase activity in the reconstituted array. A disulfide bond between the kinase and adaptor will limit the motion of the interface, effectively "stapling" it together.[33,41] If the "stapled" interface retains its native structure, it should exhibit normal function unless the disulfide prevents a structural rearrangement required for on−off switching. In that event, the formation of a disulfide across the interface may trap the native on or off state, yielding a lock-on or lock-off disulfide bond, respectively.

Only the three Cys pairs exhibiting the fastest disulfide reactions could be driven nearly to completion; thus, the analysis focused on the three resulting disulfide bonds (kD586C−aN50C, kS647C−aQ44C, and kS647C−aT46C). Arrays were assembled as before, except that prior to the first wash step, each sample was split in half. One half was oxidized with the Cu(II) catalyst under conditions that drove the disulfide formation reaction to near completion, while the other half was incubated with a reducing agent to prevent disulfide formation. Subsequently, the arrays were washed as usual, and portions were removed for the standard quantification of the

extent of disulfide-linked kinase−adaptor heterodimer formation. The remaining portions were used to quantify specific kinase activities, as described above. The amount of total kinase converted to kinase−adaptor heterodimer was ≥70% in all cases.

The three transinterface disulfide bonds each retained the ability of the array to activate and inhibit the kinase in the absence and presence of the attractant, respectively; thus, none were lock-on or lock-off disulfides. In the absence of the attractant, the three disulfide-linked arrays yielded different specific kinase activities that were (i) within error of that of the Cys-less form (kD586C−aN50C), (ii) significantly higher than that of the Cys-less form (kS647C−aQ44C), and (iii) significantly lower than that of the Cys-less form (kS647C−aT46C), as illustrated in Figure 8. Overall, these findings

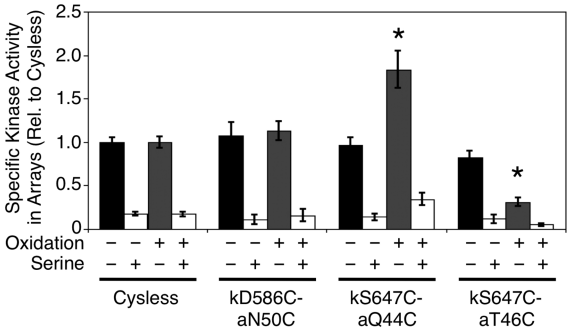

Figure 8. Effects of transinterface disulfide bonds on specific kinase activity and attractant regulation in reconstituted arrays. The three fastest-reacting di-Cys pairs were reconstituted in arrays and then subjected to strong oxidation conditions to drive disulfide formation toward completion prior to washing. The resulting arrays contained stably incorporated CheA kinase and CheW adaptor, linked by transinterface disulfide bonds. Mean final disulfide formation extents for kD586C−aN50C, kS647C−aQ44C, and aS647C−aT46C kinase−adaptor pairs were 0.71 ± 0.04, 0.87 ± 0.04, and 0.85 ± 0.04, respectively. As a control, Cys-less arrays were assembled, oxidized, and washed using the same protocol. The specific kinase activity of each cross-linked array (measured as the ratio of the total kinase activity to the total amount of kinase in the array) was normalized to the specific kinase activity of the Cys-less array in the absence of the attractant. The specific kinase activity in the presence of attractant (2 mM Ser) was determined in the same fashion. The standard error is shown for each bar, where n = 6−9. Asterisks indicate statistically significant differences relative to the Cys-less form ($p < 0.05$).

indicate that the small attractant-triggered perturbations of the interface detected by changes in disulfide formation rates (Figure 7) are small enough to be accommodated by the flexibility of the disulfide linkage, so that on−off switching can still occur. However, the sensitivity of the kinase activity to the disulfide linkages provides further support for the strong correlation between the native structure of the interface and kinase activation in the absence of the attractant.

■ DISCUSSION

The evidence provided by disulfide mapping, *in vivo* TAM-IDS analysis, and *in vitro* TAM-IDS analysis strongly supports the conclusion that the crystal structure-based (PDB entry 4JPB) threaded model accurately represents the structure of interface 1 in the kinase−adaptor ring of functional, membrane-bound chemosensory arrays (Figure 1), at least in one signaling state. This interface appears to be well-conserved across species, because the experiments are conducted on arrays formed from *E. coli* receptors and *S. typhimurium* kinase and adaptor proteins, whereas the crystal structure (PDB entry 4JPB[29]) describes the contacts among three *T. maritima* components. A similar structure of interface 1 is observed in a crystal structure of the binary *Thermatoga* complex formed between the kinase fragment and the adaptor protein (PDB entry 2CH4[15]), indicating that interface 1 has sufficient structural stability to form its native associations in the absence of other array interactions. It follows that interface 1 is highly stable and possesses one or more conserved functions in bacterial chemosensory arrays.

The remarkably strong correlation between the effects of Trp and Ala substitutions at interface 1 on (i) the stable incorporation of the kinase into the array and (ii) the specific activities of the incorporated kinase molecules in the absence of the attractant indicates that perturbations have similar effects on interface stability and kinase activation. In contrast, no such strong correlation is observed for the receptor−kinase interface previously characterized in analogous experiments.[34] Thus, the unique correlation at interface 1 provides strong evidence that this contact has dual structural and signaling functions. Specifically, the interface is crucial for both the assembly of CheA into the stable array and the activation of the array-bound kinase molecules in the absence of the attractant when the array is in its kinase-activating on state.

The attractant signal drives the array into the off state and triggers a small but significant slowing of disulfide formation across the interface, indicating that array on−off switching causes detectable changes in the structure or dynamics of the interface, yet disulfide linkages across the interface do not block this transition, providing strong support for the idea that the attractant-triggered changes are small in magnitude and can be accommodated by the intrinsic flexibility of the disulfide bond. Notably, the same mutational perturbations that impair kinase activation in the on state do not impair the downregulation of kinase activity by the attractant signal in the off state. Thus, while the stable interface contacts defined by the crystal structures and disulfide mapping are crucial to kinase activation (the on state), these contacts are not essential for attractant-triggered kinase inhibition (the off state).

Together, the evidence supports a simple model in which interface 1 must be stably associated to effectively incorporate kinase into the array and to activate the kinase, thereby explaining the strong, correlated effects of interfacial residue substitutions on kinase incorporation and specific activity in the apo on state. When the attractant binds to the receptor and switches the core unit into its off state, at least part of the interface 1 becomes less closely packed (Figure 9A). This subtle change makes packing less critical and explains why mutations affecting the interface have minimal effects on kinase inhibition in the attractant-triggered off state.

The proposed model is also consistent with the translation and/or rotation of the kinase regulatory domain previously detected in response to receptor-mediated attractant signals[34] that, in the simplest case, would be expected to perturb interface 1 packing (Figure 9B). In this model, the attractant signal displaces the receptor helix to which the kinase regulatory domain (KRD) is tightly bound, generating a translation and/or rotation of the helix−KRD unit, thereby slightly weakening interface 1.

The hypothesized signaling mechanism may represent an extension of the alternating frozen−dynamic transitions

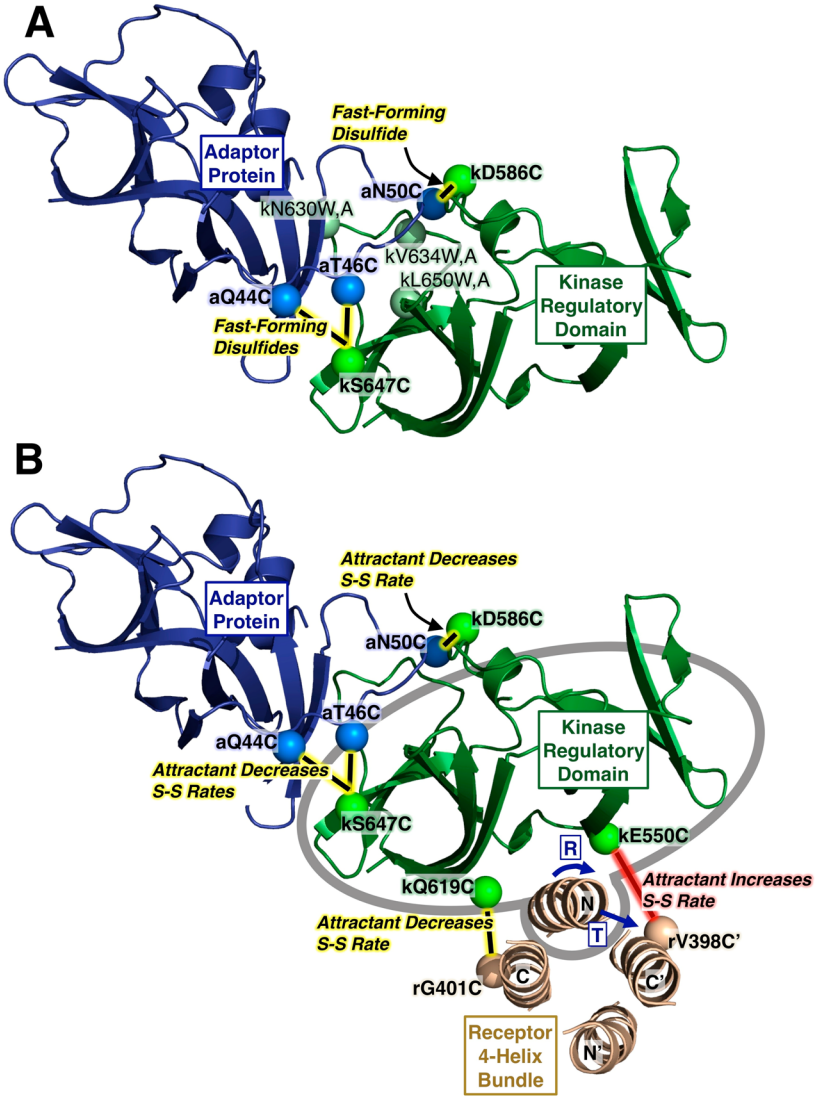

Figure 9. Model for attractant-triggered shifts at interface 1 based on attractant-triggered disulfide formation rate changes in the functional, membrane-bound array. (A) Interface 1 between the kinase regulatory domain (green) and the adaptor protein (blue) in the crystal structure-based (PDB entry 4JPB[29]) threaded model. Shown are the three fast disulfide-forming Cys pairs (β-carbon spheres connected by black lines) located at the interface. Also shown are the three interfacial Trp and Ala mutation sites (light green spheres). (B) Attractant-triggered changes in disulfide formation rates and implications for rearrangements at the receptor–kinase interface, and at kinase–adaptor interface 1. Shown again are the kinase regulatory domain and the adaptor protein, now joined by the kinase-associated hairpin region of the receptor cytoplasmic four-helix bundle (tan).[34] The kinase regulatory domain forms a tight complex with the N-terminal helix of the receptor bundle, and this complex (enclosed by a gray oval) appears to translate (T) and/or rotate (R) as a unit relative to the other helices of the receptor bundle during on–off switching as shown.[34] Two fast Cys pairs at the receptor–kinase interface exhibit attractant-sensitive disulfide formation rates that are increased (red) or decreased (black) by the attractant signal.[34] At interface 1, all three fast Cys pairs exhibit attractant-triggered rate decreases (black), consistent with a subtle decrease in the extent of close packing for at least part of the interface. The model proposes this shift at interface 1 is triggered by the translation and/or rotation at the receptor–kinase interface, assuming that the adaptor protein is anchored to a different receptor dimer (not shown; see Figure 1C).

previously found to carry attractant signals through the long receptor cytoplasmic domain to the bound kinase.[49,57,58] Kim et al. first used the term "frozen–dynamic transition" (where "frozen" is used in a relative, not literal, sense) to describe a signal-induced switch within the receptor adaptation region between a more static state and a more dynamic state,[59] as was later supported by evidence in membrane-bound receptors.[46] Subsequently, it was found that the receptor cytoplasmic domain possesses pairs of coupled, adjacent regions that exhibit alternating frozen–dynamic transitions.[49,57,58] In such pairs, when one region is more static, the adjacent region is more dynamic. On–off switching reverses the polarity of the coupled pair (for example, from frozen–dynamic to dynamic–frozen), and signals can be transmitted long distances when multiple coupled pairs are connected in series in an alternating fashion. In the receptor cytoplasmic domain, the HAMP, adaptation, and protein interaction regions are proposed to undergo alternating frozen–dynamic transitions between a kinase-activating dynamic–frozen–dynamic state and a kinase-inhibiting frozen–dynamic–frozen state.[49,57,58]

Ultimately, the alternating frozen–dynamic signal may be transmitted into the kinase–adaptor ring system, allowing the spread of the signal into the surrounding array to yield long-range cooperativity. In the on state, the local receptor four-helix bundle to which KRD is bound is in a more dynamic state,[49] allowing the kinase–adaptor ring to adopt its more stable, static

dx.doi.org/10.1021/bi401159k | *Biochemistry* 2013, 52, 7753–7765

packing arrangement. When the attractant signal switches the local receptor four-helix bundle into its more static state,[49] the displacement of the kinase regulatory domain that weakens interface 1 could drive the kinase−adaptor ring into its less well-packed but more dynamic state. Previously, studies have shown that attractant binding does not perturb the overall stability of array packing.[9] Such robust stability could indicate that when part of interface 1 is weakened by the attractant signal a different region of this interface, or a different interface in the array, is strengthened, which is conceptually similar to the previously described on−off toggling at the receptor−kinase interface.[34] Further studies are needed to test this model and to ascertain whether the subtle, attractant-triggered perturbation of interface 1 is localized within a single core unit within the array or is involved in the spread of the attractant signal to other core units in the array.

The subtle, signal-induced rearrangements proposed for interface 1 continue the pattern of low-magnitude, subtle changes detected in the transmembrane signaling domain of the receptor, the cytoplasmic domain of the receptor, and the receptor−kinase interface.[3,34,49,60] Cryo-EM studies of the array in intact cells have similarly concluded that attractant-triggered structural changes in the receptor, kinase regulatory domain, and CheW regions of the array must be small in magnitude.[61] Overall, the subtle structural and/or dynamic changes triggered in these regions by on−off switching are likely necessitated by the relatively small free energies provided by the binding of small attractant molecules (serine or aspartate for the Tsr or Tar receptor, respectively).[62] Such small free energies of binding could drive only low-energy transitions that do not greatly alter the total area or energy of the protein contacts involved in signal transmission. These energetic limitations also provide an impetus for the compensatory nature of alternating frozen−dynamic transitions proposed to carry signals through the long receptor cytoplasmic domains[49,57,58] and into the kinase−adaptor ring. In this view, as one region adopts its more dynamic state, the adjacent coupled region adopts its more stable state, yielding a net cancellation of energetic gains and losses that ensures a low-energy transition during on−off switching.

AUTHOR INFORMATION

Corresponding Author

*E-mail: falke@colorado.edu. Telephone: (303) 492-3503.

Funding

Support provided by National Institutes of Health Grant R01 GM-040731 (J.J.F.).

Notes

The authors declare no competing financial interest.

ACKNOWLEDGMENTS

We gratefully acknowledge Prof. Brian Crane (Cornell University, Ithaca, NY) for sharing coordinates prior to public release as well as Prof. Victor Sourjik, Prof. J. Sandy Parkinson, Dr. Peter Slivka, and Caleb Ulliman for helpful discussions and contributions of materials and training toward the *in vivo* TAM-IDS studies.

ABBREVIATIONS

PMSF, phenylmethanesulfonyl fluoride; YFP, yellow fluorescent protein; DTT, dithiothreitol; EDTA, ethylenediaminetetraacetic acid; SDS, sodium dodecyl sulfate; PAGE, polyacrylamide gel electrophoresis; Tris, 2-amino-2-hydroxymethylpropane-1,3-diol; TBS, Tris-buffered saline; TCEP, tris(2-carboxyethyl)phosphine; Ni-NTA, nickel-nitrilotriacetic acid-charged resin; BCA, bicinchoninic acid; PVDF, polyvinyl difluoride; NEM, *N*-ethylmaleimide; BSA, bovine serum albumin; TAM-IDS, tryptophan and alanine mutagenesis to identify docking sites; PICM, protein interactions by cysteine modification; SH3, SRC homology 3; PDB, Protein Data Bank.

REFERENCES

(1) Hazelbauer, G. L. (2012) Bacterial chemotaxis: The early years of molecular studies. *Annu. Rev. Microbiol. 66*, 285−303.

(2) Sourjik, V., and Wingreen, N. S. (2012) Responding to chemical gradients: Bacterial chemotaxis. *Curr. Opin. Cell Biol. 24*, 262−268.

(3) Hazelbauer, G. L., Falke, J. J., and Parkinson, J. S. (2008) Bacterial chemoreceptors: High-performance signaling in networked arrays. *Trends Biochem. Sci. 33*, 9−19.

(4) Chaparro, A. P., Ali, S. K., and Klose, K. E. (2010) The ToxT-dependent methyl-accepting chemoreceptors AcfB and TcpI contribute to *Vibrio cholerae* intestinal colonization. *FEMS Microbiol. Lett. 302*, 99−105.

(5) Raterman, E. L., and Welch, R. A. (2013) Chemoreceptors of *Escherichia coli* CFT073 play redundant roles in chemotaxis toward urine. *PLoS One 8*, e54133.

(6) Grim, C. J., Kozlova, E. V., Sha, J., Fitts, E. C., van Lier, C. J., Kirtley, M. L., Joseph, S. J., Read, T. D., Burd, E. M., Tall, B. D., Joseph, S. W., Horneman, A. J., Chopra, A. K., and Shak, J. R. (2013) Characterization of *Aeromonas hydrophila* wound pathotypes by comparative genomic and functional analyses of virulence genes. *MBio 4*, e00064-00013.

(7) Wuichet, K., and Zhulin, I. B. (2010) Origins and diversification of a complex signal transduction system in prokaryotes. *Sci. Signaling 3*, ra50.

(8) Briegel, A., Ortega, D. R., Tocheva, E. I., Wuichet, K., Li, Z., Chen, S., Muller, A., Iancu, C. V., Murphy, G. E., Dobro, M. J., Zhulin, I. B., and Jensen, G. J. (2009) Universal architecture of bacterial chemoreceptor arrays. *Proc. Natl. Acad. Sci. U.S.A. 106*, 17181−17186.

(9) Slivka, P. F., and Falke, J. J. (2012) Isolated Bacterial Chemosensory Array Possesses Quasi- and Ultrastable Components: Functional Links between Array Stability, Cooperativity, and Order. *Biochemistry 51*, 10218−10228.

(10) Erbse, A. H., and Falke, J. J. (2009) The core signaling proteins of bacterial chemotaxis assemble to form an ultrastable complex. *Biochemistry 48*, 6975−6987.

(11) Sourjik, V., and Berg, H. C. (2002) Receptor sensitivity in bacterial chemotaxis. *Proc. Natl. Acad. Sci. U.S.A. 99*, 123−127.

(12) Segall, J. E., Manson, M. D., and Berg, H. C. (1982) Signal processing times in bacterial chemotaxis. *Nature 296*, 855−857.

(13) Li, X., Fleetwood, A., Bilwes, A. M., Ortega, D. R., Zhulin, I. B., and Crane, B. R. (2013) The 3.2 Å resolution structure of a receptor:CheA:CheW signaling complex defines overlapping binding sites and key residue interactions within bacterial chemosensory arrays. PDB entry 4jbp.

(14) Briegel, A., Li, X., Bilwes, A. M., Hughes, K. T., Jensen, G. J., and Crane, B. R. (2012) Bacterial chemoreceptor arrays are hexagonally packed trimers of receptor dimers networked by rings of kinase and coupling proteins. *Proc. Natl. Acad. Sci. U.S.A. 109*, 3766−3771.

(15) Park, S. Y., Borbat, P. P., Gonzalez-Bonet, G., Bhatnagar, J., Pollard, A. M., Freed, J. H., Bilwes, A. M., and Crane, B. R. (2006) Reconstruction of the chemotaxis receptor-kinase assembly. *Nat. Struct. Mol. Biol. 13*, 400−407.

(16) Liu, J., Hu, B., Morado, D. R., Jani, S., Manson, M. D., and Margolin, W. (2012) Molecular architecture of chemoreceptor arrays revealed by cryoelectron tomography of *Escherichia coli* minicells. *Proc. Natl. Acad. Sci. U.S.A. 109*, E1481−E1488.

(17) Zhang, P., Khursigara, C. M., Hartnell, L. M., and Subramaniam, S. (2007) Direct visualization of *Escherichia coli* chemotaxis receptor

arrays using cryo-electron microscopy. *Proc. Natl. Acad. Sci. U.S.A. 104*, 3777−3781.
(18) Wang, X., Vu, A., Lee, K., and Dahlquist, F. W. (2012) CheA-receptor interaction sites in bacterial chemotaxis. *J. Mol. Biol. 422*, 282−290.
(19) Vu, A., Wang, X., Zhou, H., and Dahlquist, F. W. (2012) The receptor-CheW binding interface in bacterial chemotaxis. *J. Mol. Biol. 415*, 759−767.
(20) Falke, J. J., and Kim, S. H. (2000) Structure of a conserved receptor domain that regulates kinase activity: The cytoplasmic domain of bacterial taxis receptors. *Curr. Opin. Struct. Biol. 10*, 462−469.
(21) Kim, K. K., Yokota, H., and Kim, S. H. (1999) Four-helical-bundle structure of the cytoplasmic domain of a serine chemotaxis receptor. *Nature 400*, 787−792.
(22) Bilwes, A. M., Alex, L. A., Crane, B. R., and Simon, M. I. (1999) Structure of CheA, a signal-transducing histidine kinase. *Cell 96*, 131−141.
(23) Griswold, I. J., Zhou, H., Matison, M., Swanson, R. V., McIntosh, L. P., Simon, M. I., and Dahlquist, F. W. (2002) The solution structure and interactions of CheW from *Thermotoga maritima*. *Nat. Struct. Biol. 9*, 121−125.
(24) Balagopalan, L., Coussens, N. P., Sherman, E., Samelson, L. E., and Sommers, C. L. (2010) The LAT story: A tale of cooperativity, coordination, and choreography. *Cold Spring Harbor Perspect. Biol. 2*, a005512.
(25) Scarselli, M., Annibale, P., and Radenovic, A. (2012) Cell type-specific β2-adrenergic receptor clusters identified using photoactivated localization microscopy are not lipid raft related, but depend on actin cytoskeleton integrity. *J. Biol. Chem. 287*, 16768−16780.
(26) Palczewski, K. (2010) Oligomeric forms of G protein-coupled receptors (GPCRs). *Trends Biochem. Sci. 35*, 595−600.
(27) Vivo, M., Lin, H., and Strange, P. G. (2006) Investigation of cooperativity in the binding of ligands to the D_2 dopamine receptor. *Mol. Pharmacol. 69*, 226−235.
(28) Bray, D., and Duke, T. (2004) Conformational spread: The propagation of allosteric states in large multiprotein complexes. *Annu. Rev. Biophys. Biomol. Struct. 33*, 53−73.
(29) Li, X., Fleetwood, A. D., Bayas, C., Bilwes, A. M., Ortega, D. R., Falke, J. J., Zhulin, I. B., and Crane, B. R. (2013) The 3.2 Å Resolution Structure of a Receptor:CheA:CheW Signaling Complex Defines Overlapping Binding Sites and Key Residue Interactions within Bacterial Chemosensory Arrays. *Biochemistry 52*, 3852−3865.
(30) Miller, A. S., Kohout, S. C., Gilman, K. A., and Falke, J. J. (2006) CheA Kinase of bacterial chemotaxis: Chemical mapping of four essential docking sites. *Biochemistry 45*, 8699−8711.
(31) Zhao, J., and Parkinson, J. S. (2006) Cysteine-scanning analysis of the chemoreceptor-coupling domain of the *Escherichia coli* chemotaxis signaling kinase CheA. *J. Bacteriol. 188*, 4321−4330.
(32) Zhao, J., and Parkinson, J. S. (2006) Mutational analysis of the chemoreceptor-coupling domain of the *Escherichia coli* chemotaxis signaling kinase CheA. *J. Bacteriol. 188*, 3299−3307.
(33) Bass, R. B., Butler, S. L., Chervitz, S. A., Gloor, S. L., and Falke, J. J. (2007) Use of site-directed cysteine and disulfide chemistry to probe protein structure and dynamics: Applications to soluble and transmembrane receptors of bacterial chemotaxis. *Methods Enzymol. 423*, 25−51.
(34) Piasta, K. N., Ulliman, C. J., Slivka, P. F., Crane, B. R., and Falke, J. J. (2013) Defining a Key Receptor-CheA Kinase Contact and Elucidating Its Function in the Membrane-Bound Bacterial Chemosensory Array: A Disulfide Mapping and TAM-IDS Study. *Biochemistry 52*, 3866−3880.
(35) Miller, A. S., and Falke, J. J. (2004) Side chains at the membrane-water interface modulate the signaling state of a transmembrane receptor. *Biochemistry 43*, 1763−1770.
(36) Ames, P., Studdert, C. A., Reiser, R. H., and Parkinson, J. S. (2002) Collaborative signaling by mixed chemoreceptor teams in *Escherichia coli*. *Proc. Natl. Acad. Sci. U.S.A. 99*, 7060−7065.
(37) Li, G., and Weis, R. M. (2000) Covalent modification regulates ligand binding to receptor complexes in the chemosensory system of *Escherichia coli*. *Cell 100*, 357−365.
(38) Gegner, J. A., Graham, D. R., Roth, A. F., and Dahlquist, F. W. (1992) Assembly of an MCP receptor, CheW, and kinase CheA complex in the bacterial chemotaxis signal transduction pathway. *Cell 70*, 975−982.
(39) Vogel, H. J., and Bonner, D. M. (1956) Acetylornithinase of *Escherichia coli*: Partial purification and some properties. *J. Biol. Chem. 218*, 97−106.
(40) Kentner, D., Thiem, S., Hildenbeutel, M., and Sourjik, V. (2006) Determinants of chemoreceptor cluster formation in *Escherichia coli*. *Mol. Microbiol. 61*, 407−417.
(41) Chervitz, S. A., and Falke, J. J. (1995) Lock on/off disulfides identify the transmembrane signaling helix of the aspartate receptor. *J. Biol. Chem. 270*, 24043−24053.
(42) Bass, R. B., and Falke, J. J. (1999) The aspartate receptor cytoplasmic domain: In situ chemical analysis of structure, mechanism and dynamics. *Structure 7*, 829−840.
(43) Trammell, M. A., and Falke, J. J. (1999) Identification of a site critical for kinase regulation on the central processing unit (CPU) helix of the aspartate receptor. *Biochemistry 38*, 329−336.
(44) Bornhorst, J. A., and Falke, J. J. (2001) Evidence that both ligand binding and covalent adaptation drive a two-state equilibrium in the aspartate receptor signaling complex. *J. Gen. Physiol. 118*, 693−710.
(45) Mehan, R. S., White, N. C., and Falke, J. J. (2003) Mapping out regions on the surface of the aspartate receptor that are essential for kinase activation. *Biochemistry 42*, 2952−2959.
(46) Starrett, D. J., and Falke, J. J. (2005) Adaptation mechanism of the aspartate receptor: Electrostatics of the adaptation subdomain play a key role in modulating kinase activity. *Biochemistry 44*, 1550−1560.
(47) Winston, S. E., Mehan, R., and Falke, J. J. (2005) Evidence that the adaptation region of the aspartate receptor is a dynamic four-helix bundle: Cysteine and disulfide scanning studies. *Biochemistry 44*, 12655−12666.
(48) Swain, K. E., and Falke, J. J. (2007) Structure of the Conserved HAMP Domain in an Intact, Membrane-Bound Chemoreceptor: A Disulfide Mapping Study. *Biochemistry 46*, 13684−13695.
(49) Swain, K. E., Gonzalez, M. A., and Falke, J. J. (2009) Engineered socket study of signaling through a four-helix bundle: Evidence for a yin-yang mechanism in the kinase control module of the aspartate receptor. *Biochemistry 48*, 9266−9277.
(50) Kelley, L. A., and Sternberg, M. J. (2009) Protein structure prediction on the Web: A case study using the Phyre server. *Nat. Protoc. 4*, 363−371.
(51) Gloor, S. L., and Falke, J. J. (2009) Thermal domain motions of CheA kinase in solution: Disulfide trapping reveals the motional constraints leading to trans-autophosphorylation. *Biochemistry 48*, 3631−3644.
(52) Bers, D. M., Patton, C. W., and Nuccitelli, R. (2010) A practical guide to the preparation of Ca^{2+} buffers. *Methods Cell Biol. 99*, 1−26.
(53) Borkovich, K. A., Kaplan, N., Hess, J. F., and Simon, M. I. (1989) Transmembrane signal transduction in bacterial chemotaxis involves ligand-dependent activation of phosphate group transfer. *Proc. Natl. Acad. Sci. U.S.A. 86*, 1208−1212.
(54) Ninfa, E. G., Stock, A., Mowbray, S., and Stock, J. (1991) Reconstitution of the bacterial chemotaxis signal transduction system from purified components. *J. Biol. Chem. 266*, 9764−9770.
(55) Hughson, A. G., and Hazelbauer, G. L. (1996) Detecting the conformational change of transmembrane signaling in a bacterial chemoreceptor by measuring effects on disulfide cross-linking in vivo. *Proc. Natl. Acad. Sci. U.S.A. 93*, 11546−11551.
(56) Falke, J. J., and Koshland, D. E., Jr. (1987) Global flexibility in a sensory receptor: A site-directed cross-linking approach. *Science 237*, 1596−1600.
(57) Zhou, Q., Ames, P., and Parkinson, J. S. (2011) Biphasic control logic of HAMP domain signalling in the *Escherichia coli* serine chemoreceptor. *Mol. Microbiol. 80*, 596−611.

(58) Zhou, Q., Ames, P., and Parkinson, J. S. (2009) Mutational analyses of HAMP helices suggest a dynamic bundle model of input-output signalling in chemoreceptors. *Mol. Microbiol. 73*, 801−814.
(59) Kim, S. H. (1994) "Frozen" dynamic dimer model for transmembrane signaling in bacterial chemotaxis receptors. *Protein Sci. 3*, 159−165.
(60) Falke, J. J., and Hazelbauer, G. L. (2001) Transmembrane signaling in bacterial chemoreceptors. *Trends Biochem. Sci. 26*, 257−265.
(61) Briegel, A., Beeby, M., Thanbichler, M., and Jensen, G. J. (2011) Activated chemoreceptor arrays remain intact and hexagonally packed. *Mol. Microbiol. 82*, 748−757.
(62) Falke, J. J., Bass, R. B., Butler, S. L., Chervitz, S. A., and Danielson, M. A. (1997) The two-component signaling pathway of bacterial chemotaxis: A molecular view of signal transduction by receptors, kinases, and adaptation enzymes. *Annu. Rev. Cell Dev. Biol. 13*, 457−512.